Research Article

Examination of Perovskite Structure CaMnO$_{3-\delta}$ with MgO Addition as Oxygen Carrier for Chemical Looping with Oxygen Uncoupling Using Methane and Syngas

Dazheng Jing,[1] Tobias Mattisson,[2] Henrik Leion,[1] Magnus Rydén,[2] and Anders Lyngfelt[2]

[1] *Department of Chemical and Biological Engineering, Division of Environmental and Inorganic Chemistry, Chalmers University of Technology, 41296 Gothenburg, Sweden*

[2] *Department of Energy and Environment, Division of Energy Technology, Chalmers University of Technology, 41296 Gothenburg, Sweden*

Correspondence should be addressed to Dazheng Jing; dazheng@chalmers.se

Perovskite structure oxygen carriers with the general formula CaMn$_x$Mg$_{1-x}$O$_{3-\delta}$ were spray-dried and examined in a batch fluidized bed reactor. The CLOU behavior, reactivity towards methane, and syngas were investigated at temperature 900°C to 1050°C. All particles showed CLOU behavior at these temperatures. For experiments with methane, a bed mass corresponding to 57 kg/MW was used in the reactor, and the average CH$_4$ to CO$_2$ conversion was above 97% for most materials. Full syngas conversion was achieved for all materials utilizing a bed mass corresponding to 178 kg/MW. SEM/EDX and XRD confirmed the presence of MgO in the fresh and used samples, indicating that the Mg cation is not incorporated into the perovskite structure and the active compound is likely pure CaMnO$_{3-\delta}$. The very high reactivity with fuel gases, comparable to that of baseline oxygen carriers of NiO, makes these perovskite particles highly interesting for commercial CLC application. Contrary to NiO, oxygen carriers based on CaMnO$_{3-\delta}$ have no thermodynamic limitations for methane oxidation to CO$_2$ and H$_2$O, not to mention that the materials are environmentally friendly and can utilize much cheaper raw materials for production. The physical properties, crystalline phases, and morphology information were also determined in this work.

1. Introduction

Carbon dioxide is the greenhouse gas which contributes most to anthropogenic climate change. A significant amount of CO$_2$ is emitted into the atmosphere each year, of which combustion of fossil fuels was responsible for over 30000 million tons of CO$_2$ in 2010 [1]. The increasing energy demand of a globally growing economy will likely make fossil fuels the main energy source in the foreseeable future. Hence, reducing CO$_2$ emission from combustion of fossil fuels is a key point in reducing the impact of global warming.

CO$_2$ capture and storage (CCS) is one important option to reduce CO$_2$ emission. In this concept, CO$_2$ produced from combustion or industrial processes is captured and stored in closed geological formations where it is stored for long periods of time before being converted to carbonate minerals or other stable phases by natural processes. Some of the carbon dioxide may actually leak to the atmosphere, but if the leakage rate is low enough, this may not be of significant importance as natural mechanisms could sequester the carbon. CO$_2$ capture can be achieved by different technologies and the most discussed are postcombustion, precombustion and oxyfuel combustion. Unfortunately, a substantial energy penalty is required for gas separation in these technologies [2]. Chemical-looping combustion is a process of burning fuel where the air and fuel are never mixed and where CO$_2$ is inherently separated from the rest of the flue gases without any direct energy expenditure. There has been a

Oxygen depleted air CO_2, H_2O

Me_xO_y

Air reactor   Fuel reactor
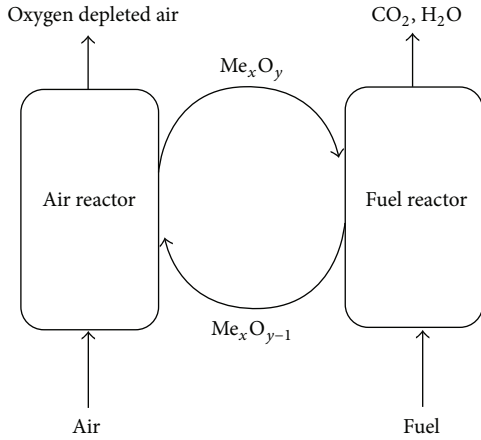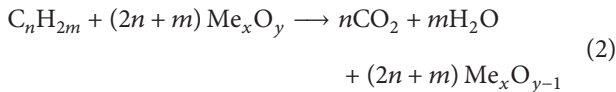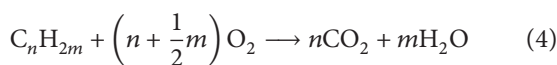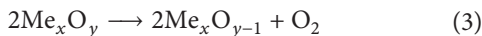
Me_xO_{y-1}

Air   Fuel

FIGURE 1: Schematic representation of a CLC unit.

strong interest for this technology in the last decade, as judged by the number of research groups working in the field and the number of scientific articles published [3, 4].

Chemical-looping combustion is an innovative combustion technology in which there is no direct contact between combustion air and fuel. A chemical-looping combustion unit consists of two reactors, an air reactor and a fuel reactor; see Figure 1 [5]. Solid oxygen carriers, which are usually metal oxide particles, are oxidized in the air reactor according to reaction (1) and circulated to the fuel reactor, where they are reduced by the fuel according to reaction (2). The oxygen needed for fuel conversion is supplied by the solid oxygen carrier particles. The reduced particles are recirculated to the air reactor and the process is repeated. The heat produced by CLC is the same as a conventional combustion which is revealed by combining reaction (1) and (2). After steam condensation, high purity CO_2 ready for compression and storage is obtained after the fuel reactor. By transferring oxygen by solid oxygen carriers, the combustion products are not diluted with N_2 from the air. Thus the energy required for gas separation is avoided. Also, the CO_2 capture efficiency can reach 100% in chemical-looping combustion [6, 7]. These unique features make chemical-looping combustion a very interesting option for CO_2 capture

$$O_2 + 2Me_xO_{y-1} \longrightarrow 2Me_xO_y \qquad (1)$$

$$C_nH_{2m} + (2n + m)\, Me_xO_y \longrightarrow nCO_2 + mH_2O$$
$$+ (2n + m)\, Me_xO_{y-1} \qquad (2)$$

In the fuel reactor, some kinds of oxygen-carrier materials are able to release gaseous oxygen according to reaction (3). In a subsequent step, the fuel reacts directly with the released oxygen according to reaction (4). Such a process is referred to as chemical-looping with oxygen uncoupling (CLOU) [8]. Oxygen carriers with the ability to release gas phase O_2 are referred to as CLOU materials

$$2Me_xO_y \longrightarrow 2Me_xO_{y-1} + O_2 \qquad (3)$$

$$C_nH_{2m} + \left(n + \frac{1}{2}m\right)O_2 \longrightarrow nCO_2 + mH_2O \qquad (4)$$

Oxygen carriers are most often based on metal oxides, which can be cyclically oxidized and reduced when exposed to different environments. For a metal oxide to be an oxygen carrier and the CLC process to be operationally feasible with high CO_2 capture efficiency, certain properties of a material are required.

(a) Suitable thermodynamic and kinetic properties under combustion conditions. This means that materials can be oxidized and reduced at relevant conditions with sufficient reaction rates. The reactivity towards fuels should be high in CLC, and the rate of oxygen release should be high in the CLOU process.

(b) The performance of an oxygen carrier should be stable in long-term operation.

(c) When using fluidized beds for both the air and the fuel reactor, good fluidizing properties are required, for example, the particles should not form agglomerations.

(d) Resistance against attrition and mechanical strength should be high.

(e) The oxygen carrier should be environmental friendly and have reasonable costs.

Mn, Cu, Ni, Co, Cd, and their corresponding oxides have been proposed as possible oxygen carrier candidates [9–11]. Among a large number of studied oxygen carriers, NiO-based oxygen carrier has been successfully demonstrated in 10 kW [12] and 120 kW CLC units [13]. In the 10 kW unit, a NiO-based material has been operated more than 1000 h achieving high CH_4 conversion and very low loss of fines, corresponding to over 30 000 h life time [12]. Considering the good experience obtained with Ni-based oxygen carriers with respect to reactivity and stability with gaseous fuels, at present NiO could be considered to be the baseline CLC oxygen carrier. However, Ni-based materials have some important disadvantages, most critically being the high toxicity. In addition, Ni is expensive and has a negative equilibrium restraint for fuel conversion [14]. For CLOU materials, CuO has been investigated extensively [8, 15–19]. Although Cu-based oxygen carriers in general seem to have very high rates of oxygen uncoupling, copper is also fairly expensive, and there have been problems reported related to agglomeration and stability [20–22]. For uplifting chemical-looping combustion to the next scale application, developing new materials with lower cost than Ni and Cu but with CLOU properties would be of significant value.

Theoretically, Mn_2O_3 is capable of releasing oxygen in the fuel reactor during chemical-looping combustion. But the oxidation of Mn_3O_4 to Mn_2O_3 is thermodynamically hindered at temperatures above ≈800°C. At lower temperatures, where there are no thermodynamic limitations, the oxidation of Mn_3O_4 to Mn_2O_3 is hard to achieve, probably due to kinetic limitations [23]. One option to improve the thermodynamic and kinetic properties of manganese oxides is to combine them with other metal oxides forming combined oxide systems. Mn-Fe combined oxides were studied by Azimi et al. [24, 25], Rydén et al. [26], and Shulman et

TABLE 1: Composition of Ca-Mn-Mg oxygen carriers.

Notation	Molar composition	Synthesis composition (wt%)	Sintering temperature (°C)	Sintering time (h)
5.6% MgO	$CaMn_{0.8}Mg_{0.2}O_3$	42.6% Mn_3O_4 51.8% $Ca(OH)_2$ 5.6% MgO	1100, 1200, 1300	4
2.7% MgO	$CaMn_{0.9}Mg_{0.1}O_3$	46.8% Mn_3O_4 50.5% $Ca(OH)_2$ 2.7% MgO	1100, 1200, 1300	4

al. [27] showing that such oxides had CLOU capability and rapid oxidation rate at 850°C. Jing et al. [28] have studied the Mn-Si combined oxide system and CLOU behavior; high methane and syngas conversion were reported. Rydén et al. [29] provided an overview of six combined manganese oxides systems which have been studied so far with respect to CLOU, and Mattisson has provided a general overview of CLOU materials [30].

One of the more interesting combined oxides is the perovskite structure calcium manganite, or $CaMnO_{3-\delta}$. This type of materials is of defect perovskite structure with general formula $ABO_{3-\delta}$. In such a structure, the oxygen deficiency δ can vary depending on the surrounding oxygen partial pressure or temperature [31, 32]. When the surrounding oxygen partial pressure decreases, the defect grows by releasing oxygen according to reaction (5), and this oxygen can be utilized by the fuel in accordance with the CLOU process described above

$$2ABO_{3-\delta} \longrightarrow 2ABO_{3-\delta-a} + aO_2 \qquad (5)$$
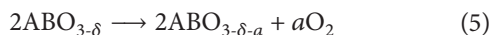
Another promising feature of such materials is that there is no distinct phase transition between oxidized $ABO_{3-\delta}$ and reduced $ABO_{3-\delta-a}$. This may be advantageous and may help in avoiding the attrition problem caused by structural changes between oxidized and reduced phase. $CaMn_{0.875}Ti_{0.125}O_3$ has been examined in TGA, batch fluidized reactor, and small scale fluidized bed reactor showing good CLOU properties, high reactivity towards methane, and good fluidization behavior by Leion et al. [33] and Rydén et al. [34] Another set of $CaMn_{(1-x)}M_xO_{3-\delta}$ (M = Ti, Fe, Mg) materials with good reactivity results and CLOU properties were examined by Hallberg et al. [35] using a batch fluidized bed reactor system. Here, it was found that a calcium manganite material doped with MgO showed the most promising performance.

2. Objective

In the previous screening work of $CaMn_{(1-x)}M_xO_{3-\delta}$ (M = Ti, Fe, Mg) materials [35], $CaMn_{(1-x)}Mg_xO_{3-\delta}$ with 2.7 wt% and 5.6 wt% MgO exhibited CLOU behavior and high methane conversion at 950°C. These two materials were selected and their performance was further examined. The ability to release gas phase oxygen and the reactivity towards methane and syngas at different temperatures as well as the stability over many red-ox cycles were investigated. Also, physical and chemical properties, for instance the crushing strength and

the crystalline phases, of the oxygen carrier particles were analyzed.

3. Experimental Section

3.1. Manufacture of Oxygen Carriers. The oxygen carriers examined in this work were manufactured by VITO, Belgium, using spray-drying. Spray-drying is an industrial process for producing high spherical, free-flowing, homogeneous granulated powder of uniform bulk density. Inorganic raw materials $Ca(OH)_2$, Mn_3O_4, and MgO were weighed and dispersed in deionized water with appropriate amounts of organic binders and dispersants. The water based suspension was homogenized by milling in a planetary ball mill. The slurry was continuously stirred with a propeller blade mixer while being pumped into an atomizer which was located in the drying chamber. Under the effects of surface tension, the pumped slurry was broken into a large number of droplets which quickly dried by heated air due to a large surface-to-volume ratio of the droplets thus transformed rapidly into dry powders and separated from the hot air. The particles synthesized were sieved and sintered at 1100°C, 1200°C, or 1300°C for 4 h in air to obtain sufficient mechanical strength. Oxygen carriers in the diameter range 125–180 μm were selected for reactivity testing and 180–212 μm for crushing strength (CS) measurements. The compositions of the examined oxygen carriers are presented in Table 1. In the screening work of Hallberg et al. [35], the 5.6% MgO and 2.7% MgO oxygen carriers were presented as C13 and C14, respectively. Källén et al. [36] used $CaMn_{0.9}Mg_{0.1}O_3$ to notate the 2.7% MgO material which was used in continuous operation.

3.2. Characterization of Oxygen Carriers. The hardness of an oxygen carrier is measured by the force needed to fracture a particle and is typically referred to as crushing strength (CS) [37]. In this work, crushing strength was measured with a Shimpo FNG-5 apparatus on fresh particles with diameter 180–212 μm. 30 particles were measured for each sample, and the average value is given as the CS for the sample.

The chemical compositions and crystalline structures of the oxygen carriers were identified by X-ray powder diffraction using a Siemens D5000 diffractometer utilizing copper Kα_1 radiation. Light microscopy and scanning electron microscopy (SEM), FEI Quanta 200 Environmental, were used to provide morphology information of the materials. With the help of an Oxford Inca Energy dispersive X-ray

TABLE 2: Experimental scheme for oxygen carriers' reactivity test.

No. of cycles	Inert/reducing gas	t_{CLOU} (s)	t_{In} (s)	t_{Red} (s)	T_{Ox} (°C)	T_{Red}/T_{CLOU} (°C)
3	Nitrogen[a]	360			900	900
3	Methane		60	20	950	950
3	Syngas		60	80	950	950
3	Nitrogen	360			900	900
1	Nitrogen	1800			900	1000

[a]The oxygen concentration was measured during the inert periods in order to evaluate the ability of the oxygen carriers' to release oxygen in the gas phase.

system (EDX) attached to SEM, the elemental composition on particles' surface was obtained.

3.3. Batch Fluidized Bed Reactor System. The reactivity tests were conducted in a quartz fluidized bed reactor with total length of 870 mm and inner diameter of 22 mm. A porous plate supporting bed material was placed 370 mm from the bottom. The temperature was measured 25 mm above and 5 mm underneath the porous plate by Pentronic CrAl/NiAl thermocouples enclosed in inconel-600 alloys inside quartz shells. Honeywell pressure transducers with 20 Hz frequency was used to measure the pressure drop over the particle bed and the porous plate.

A specified amount of oxygen carrier with diameter 125–180 μm was placed on the porous plate for the reactivity test. Initially, the particles were heated to the reaction temperature in a gas mixture of 5% O_2 in N_2. The reacting gases were then introduced from the bottom of the reactor. Flue gases leaving from the top of the reactor were cooled by an electric cooler. After condensation of water, the concentrations of CO, CO_2, CH_4, and O_2, as well as the volume flow of the dry gas, were measured with a Rosemount NGA-2000 gas analyzer. Figure 2 is a schematic representation of the reactor system. The same system has been used previously by Jerndal et al. [37], Arjmand et al. [17], Azimi et al. [24, 25], Shulman et al. [27], Jing et al. [28], Sundqvist et al. [38], and Hallberg et al. [35].

3.4. Reactivity Tests

3.4.1. Uncoupling Properties and Reactivity with CH_4 and Syngas. A sample of 15 g oxygen carrier with diameter 125–180 μm was placed in the quartz reactor and was then heated from room temperature to 900°C in 5% O_2. Table 2 outlines the experimental scheme. Firstly, three inert cycles were performed by exposing the particles alternatingly to 100% N_2 and 5% O_2 at 900°C. By measuring the oxygen concentration during such inert cycles, the oxygen carriers CLOU property could be examined. Subsequently, the particles were exposed to three methane cycles and three syngas (50% CO and 50% H_2) cycles at 950°C. Then, three more inert cycles were carried out at 900°C. Afterwards, one 1800 s inert cycle was performed at 1000°C to calculate the materials' oxygen capacity with respect to CLOU. Finally, the oxygen carriers

were cooled down to room temperature during fluidization with 5% O_2. The gas flows applied were 900 mL_N/min for 5% O_2 (in N_2), 600 mL_N/min for N_2, and 450 mL_N/min for CH_4 and syngas. These flows correspond to 8–28 u_{mf} in the oxidation period and 3–9 u_{mf} in the reduction period. The experimental procedure, with the injection time for N_2 and fuel, is stated in Table 2 for different cycles. N_2 was used to flush the reactor for 60 s before and after fuel introduction to prevent back mixing.

3.4.2. Temperature Influence on Oxygen Carriers' Reactivity. The effect of temperature on the performance of oxygen carrier was studied by conducting cyclic reactivity tests in the batch fluidized reactor. As can be seen from Table 3, the experiments started at 900°C followed by cycles at 950°C, 1000°C, and 1050°C. Finally, the temperature was reduced to 950°C. The last test was made in order to judge if the redox cycles at higher temperatures had any permanent effect on the particle reactivity behavior. At each temperature, two methane reduction cycles and two inert cycles were carried out, as seen in the table. As before, 15 g of fresh sample was used in this series of tests. After the cycles the material was cooled down to room temperature in 600 mL_N/min 100% N_2. Gas flows were the same as those used for the experiments described in Section 3.4.1.

3.4.3. Investigation of Reactivity Stability and Reduction Time. The reactivity over many redox cycles was also investigated in this work. A sample of 2 g of $CaMn_{0.8}Mg_{0.2}O_3$ sintered at 1300°C (short for 5.6% MgO 1300) which had previously been used in general reactivity screening was placed in the quartz reactor. The particles were exposed alternately to 10% O_2 in N_2, 100% N_2 and pure CH_4. The inlet flows were 900 mL_N/min for all components. As seen in Table 4, two sets of experiments were done, with the methane injection period set to 2 s and 14 s, respectively, for the different experiments. A total of 50 cycles were conducted for each experiment.

3.5. Data Evaluation. Fuel conversion, or fuel yield, is defined as a degree of how much introduced fuel has been fully converted into CO_2. It is used to quantify an oxygen carrier's reactivity towards fuels. Methane and syngas conversion are
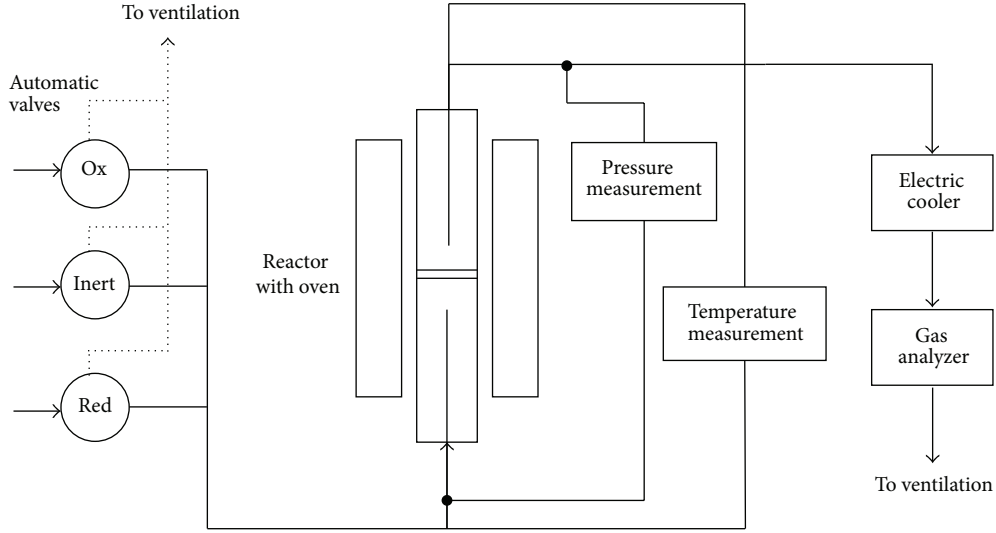
FIGURE 2: Schematic representation of the laboratory set-up of the batch fluidized bed system.

TABLE 3: Experimental scheme used for investigation of the effect of temperature on the oxygen carrier reactivity.

No. of cycles	Inert/reducing gas	t_{CLOU} (s)	t_{In} (s)	t_{Red} (s)	T_{Ox} (°C)	T_{Red}/T_{CLOU} (°C)
2	Methane		60	20	900	900
2	Nitrogen	360			900	900
2	Methane		60	20	950	950
2	Nitrogen	360			950	950
2	Methane		60	20	1000	1000
2	Nitrogen	360			1000	1000
2	Methane		60	20	1050	1050
2	Nitrogen	360			1050	1050
2	Methane		60	20	950	950
2	Nitrogen	360			950	950

TABLE 4: Experimental scheme for stability tests.

Sample batch	No. of cycles	Reducing gas	t_{In} (s)	t_{Red} (s)	T_{Ox} (°C)	T_{Red} (°C)
1	50	Methane	60	2	950	950
2	50	Methane	60	14	950	950

presented as (6) showing the CH_4 and CO conversion to CO_2 respectively

$$\gamma_{CH_4} = \frac{p_{CO_2}}{p_{CO_2} + p_{CO} + p_{CH_4}},$$

$$\gamma_{syn} = \frac{p_{CO_2}}{p_{CO_2} + p_{CO}}, \qquad (6)$$

where p_i is the outlet partial pressure of component i.

Oxygen carrier conversion (or solid conversion) is defined as

$$\omega_i = \frac{m_i}{m_{ox}}, \qquad (7)$$

where m_i is the mass of the oxygen carrier at time i and m_{ox} is the mass of the fully oxidized oxygen carrier. Here, m_{ox} is simply the mass of the fresh particles used in the experiments, and no account has been taken to the possible oxygen deficiency at higher temperatures [29]. In a fuel reduction period, ω_i can also be calculated as a function of time. Equation (8) shows the oxygen carrier conversion during a methane and syngas reduction period, respectively, as follows:

$$\omega_i = \omega_{i-1} - \int_{t_{i-1}}^{t_i} \frac{\dot{n}_{out}M_o}{m_{ox}P_{tot}} \left(4p_{CO_2,out} + 3p_{CO,out} - p_{H_2,out}\right) dt,$$

$$\omega_i = \omega_{i-1} - \int_{t_{i-1}}^{t_i} \frac{\dot{n}_{out}M_o}{m_{ox}P_{tot}} \left(2p_{CO_2,out} + p_{CO,out} - p_{H_2,out}\right) dt,$$

$$(8)$$

where $\dot{n}_{out}$ is the molar flux of flue gas after water condensation and M_o is the molar mass of oxygen. For a specific reduction cycle, γ_{CH_4}, is sometimes given as an average value from $\omega = 1$ to 0.99. The concentration of H_2 was not measured during experiments. H_2 concentration can

be assumed to be low enough to be neglected since H_2 generally has a higher reactivity than CO [39] and the CO concentration was very low under all conditions.

4. Results

4.1. Crushing Strength and Effective Density. The crushing strengths and effective densities of the calcium manganite oxygen carriers are presented in Table 5. Effective density is calculated from measurement of the volume and mass of a small bed of particles. By assuming a void fraction of 0.37, the effective density can be calculated as

$$\text{Effective density} = \frac{m_{\text{solids}}}{V_{\text{solids}} * (1 - 0.37)}. \tag{9}$$

Figure 3 shows the crushing strength and effective density versus sintering temperature. Obviously, particles sintered at higher temperature are denser and have higher mechanical strength. Oxygen carriers with higher crushing strength are likely preferred in CLC since it may indicate a reasonable resistance against attrition and fragmentation. But particles with high density may be more prone to defluidization, especially at low velocities. The crushing strengths of the samples sintered at 1100°C were judged to be too low, and these samples were excluded from batch reactor testing.

4.2. General Screening of Oxygen Carriers' Reactivity

4.2.1. CLOU Property at 900°C and 1000°C. The ability of oxygen carrier particles to release oxygen in the gas phase, or the so-called oxygen uncoupling properties, was investigated by exposing the particles to inert periods both before and after fuel cycles; see Table 2. By gauging the difference in oxygen uncoupling properties from before and after fuel testing, it is possible to see if the particles become deactivated during the exposure to fuel. Figure 4(a) shows the oxygen concentration profile of 7 inert cycles tested at 900°C on the sample with 5.6% MgO, sintered at 1300°C. Here, 3 cycles are conducted before exposure to fuel (solid lines), 3 cycles are taken after exposure to fuel (dashed lines), and 1 blank reference cycle is included. In the reference, 15 g of inert silica sand was used in the bed, and the air was switched to inert in the same way as when the oxygen carrier particles were bed material. Of course, no uncoupling properties are expected from this reference experiment.

At $t = 0$ s in Figure 4(a), 100% N_2 was injected to the system instead of 5% O_2. Due to a delay in the measuring system, oxygen concentration stays at 5% for the first 20 s. For a material without CLOU property, for instance, the sand reference, the oxygen concentration drops sharply to 0 as shown by the reference plot. On the other hand, the sample, 5.6% MgO 1300, releases gaseous oxygen yielding the smooth gradually decreased oxygen concentration. It can be seen from the figures that the materials exhibit stable uncoupling properties as a function of time for the first three cycles. The reactivity is somewhat less after the fuel cycles, but in general there seems to be very little deactivation caused by the exposure to fuel. The amount of oxygen removed

by the uncoupling reactions after 360 s corresponded to approximately 0.5 wt% of the total mass of oxygen carrier.

To be able to calculate the oxygen uncoupling capacity of the oxygen carrier particles, one 1800 s inert cycle was performed at 1000°C. Here, the oxidation was carried out at 900°C, but the temperature was increased to 1000°C during the oxidation. Figure 4(b) presents the oxygen concentration profile of the 1800 s inert cycle performed on 5.6% MgO 1300 sample. The small peak at around $t = 175$ s resulted from the temperature increase to 1000°C. At the end of the cycle, the concentration of uncoupled oxygen was almost zero indicating that little oxygen was available for CLOU. By integrating the concentration difference between blank reference and tested sample, the material's CLOU oxygen capacity is estimated to about 1 wt%.

Table 6 summarizes the data for the CLOU experiments at 900°C. Here, the concentration of O_2 after 360 s is given, averaged for the three cycles before and after fuel cycles. Clearly, there is a decreased CLOU activity following the fuel cycles. For the 5.6% MgO 1200 sample, the O_2 concentration after the fuel cycles dropped 0.1%-unit compared with the concentration before fuel cycles. This may be due to some physical or chemical deactivation in the fuel cycles; for instance, it is possible that other phases besides the calcium manganite is formed during the reduction, for instance, $CaMn_2O_4$ or Ca_2MnO_4, which could affect the reactivity [32].

4.2.2. Reactivity of Oxygen Carriers towards Fuels at 950°C. All investigated oxygen carriers exhibited high reactivity towards gaseous fuels. Methane conversion of over 97% and full conversion of syngas were achieved for all samples. Figure 5 shows the dry flue gas concentration profile of the second methane cycle at 950°C performed on sample 5.6% MgO 1300. At $t = 0$ s, 5% O_2 was switched off and N_2 was injected for 60 s. The O_2 concentration in the reactor drops immediately after around $t = 20$ s, a lag time which is due to the system delay, however remaining at around 1.5% at the end of inert step resulting from the CLOU behavior of the oxygen carrier. At $t = 60$ s, the N_2 flow was turned off and methane was switched on for 20 s. Inlet methane was immediately converted to CO_2, and the high reactivity of the material gives a high and sharp CO_2 peak. In Figure 5, the breakthrough of CO_2 does not come until about $t = 80$ s, once again due to the time delay in the system. Flushing of N_2 is seen at $t = 100$ s in Figure 5, after which the concentrations of detected gaseous species decrease to zero rapidly.

Figure 6 presents the methane yield versus solid conversion for all 4 samples. The second methane reduction cycle was selected for comparison. At the beginning of reduction, injected methane was fully converted into CO_2 giving full conversion for all samples. As reduction proceeds, less oxygen becomes available in the oxygen carrier. So the material becomes less reactive, which is logical considering that the equilibrium partial pressure of O_2 becomes less at higher degrees of reduction, and thus likely also the release rate. Since less oxygen is available for methane conversion, this may be the reason of the increased methane concentration from $t = 90$ s to $t = 100$ s in Figure 5. This leads to the slightly
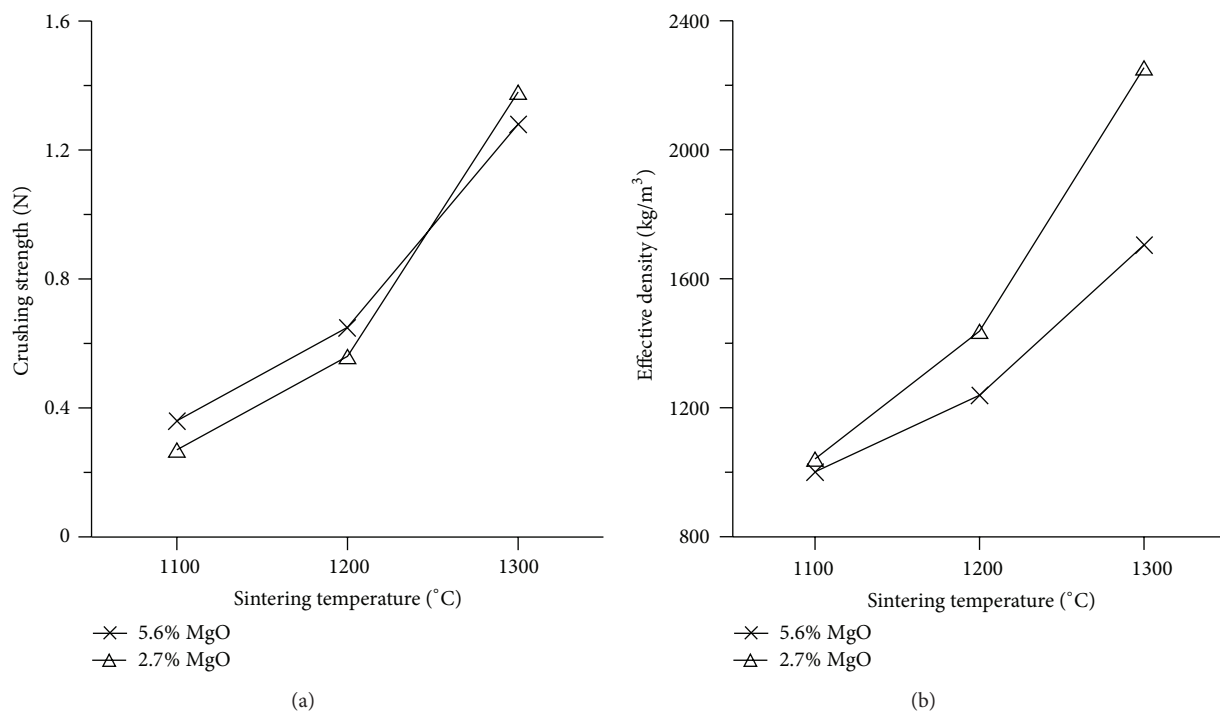
FIGURE 3: Crushing strength (a) and effective density (b) as a function of sintering temperature for all investigated particles.
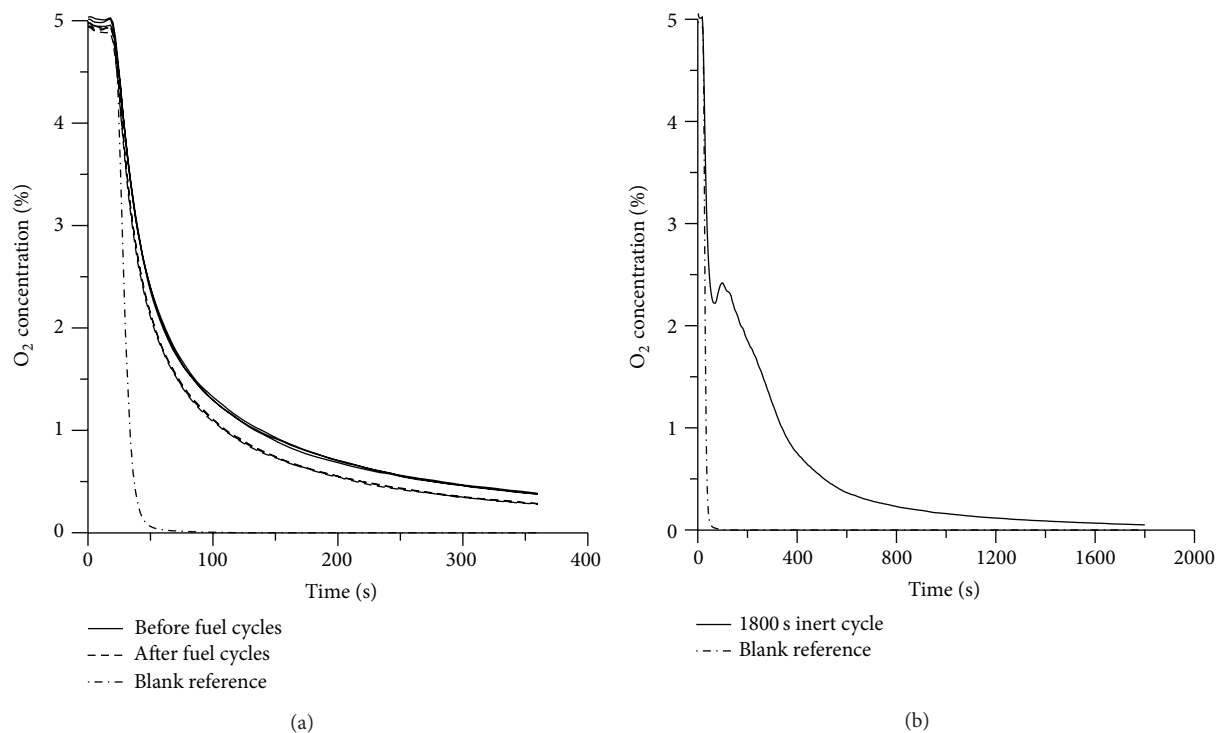

FIGURE 4: O_2 concentration profile in inert cycles. Tests were carried out on the 5.6% MgO 1300 sample. (a) inert cycles at 900°C; (b) 1800 s inert cycle at 1000°C. For the experiments in Figure 4(a), three cycles were conducted before and following the fuel cycles. In Figure 4(b), the oxidation was performed at 900°C

TABLE 5: Crushing strength and effective density of MgO added $CaMnO_{3-\delta}$ materials.

Notation	Molar composition	Sintering temperature (°C)	Crushing strength (N)	Effective density (kg/m^3)
5.6% MgO	$CaMn_{0.8}Mg_{0.2}O_3$	1100	0.4	1001.2
		1200	0.7	1238.7
		1300	1.3	1704.9
2.7% MgO	$CaMn_{0.9}Mg_{0.1}O_3$	1100	0.3	1041.3
		1200	0.6	1437.6
		1300	1.4	2254.6

TABLE 6: Oxygen concentration at the end of the CLOU period for tested oxygen carrier particles.

Notation	Molar composition	Sintering temperature (°C)	Conc. (O_2) end of inert ($T = 900$°C)	
			Before fuel (%)	After fuel (%)
5.6% MgO	$CaMn_{0.8}Mg_{0.2}O_3$	1200	0.5	0.1
		1300	0.4	0.3
2.7% MgO	$CaMn_{0.9}Mg_{0.1}O_3$	1200	0.5	0.3
		1300	0.5	0.4
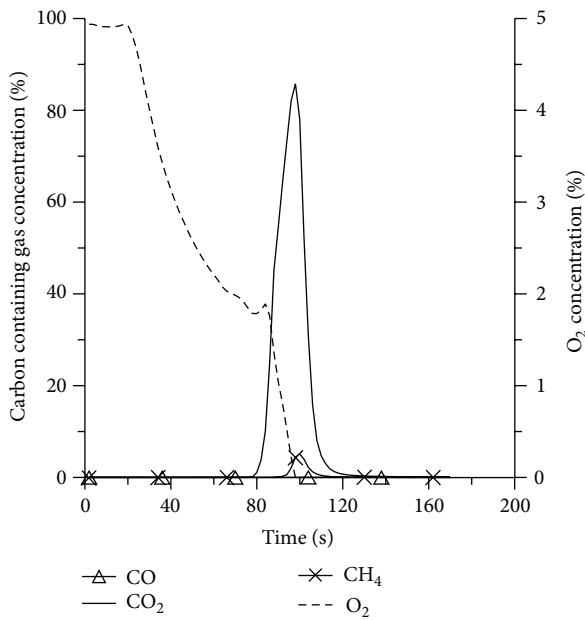
FIGURE 5: Dry gas concentration profile of the second methane cycle at 950°C on the 5.6% MgO 1300 sample.
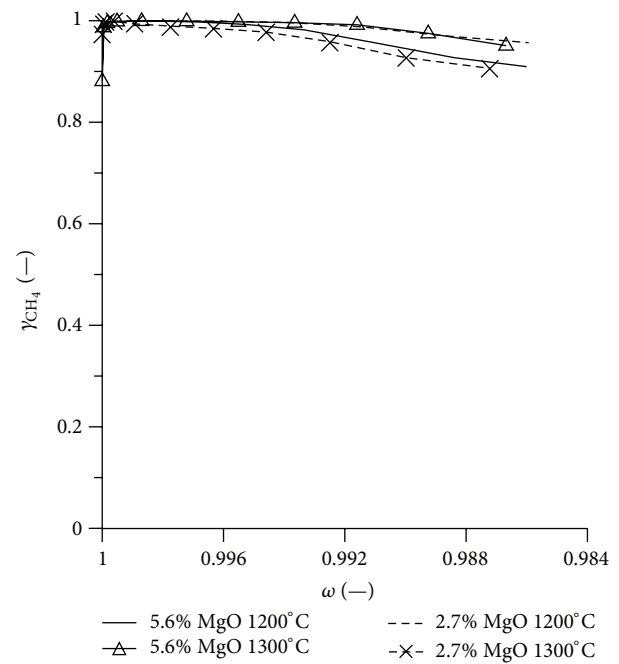
FIGURE 6: Methane yield as a function of solid conversion of the second methane cycle at 950°C.

decrease of methane conversion at the end of the reduction. Still the material has very high reactivity throughout the reduction period, exceeding 97% in the ω range 1 to 0.99.

Figures 7 and 8 demonstrate the dry gas concentration profile and syngas yield as a function of solid conversion for tested samples. Syngas consisting 50% CO and 50% H_2 is apparently easier to oxidize, as compared with methane. Another factor is the fact that syngas needs less oxygen per mole fuel in order to be converted to CO_2 and H_2O. So there

was complete syngas conversion, that is, for ω from 1 to 0.99, for all samples.

4.3. Influence of Temperature on the Reactivity of the Oxygen Carriers. The methane yield as a function of solid conversion at different temperatures is presented in Figure 9 for the particles 5.6% MgO 1300. In Figure 9(b), which compares the reactivity at 950°C, before and after testing at 1050°C, "1" indicates the temperature before 1050°C cycles, and "2"
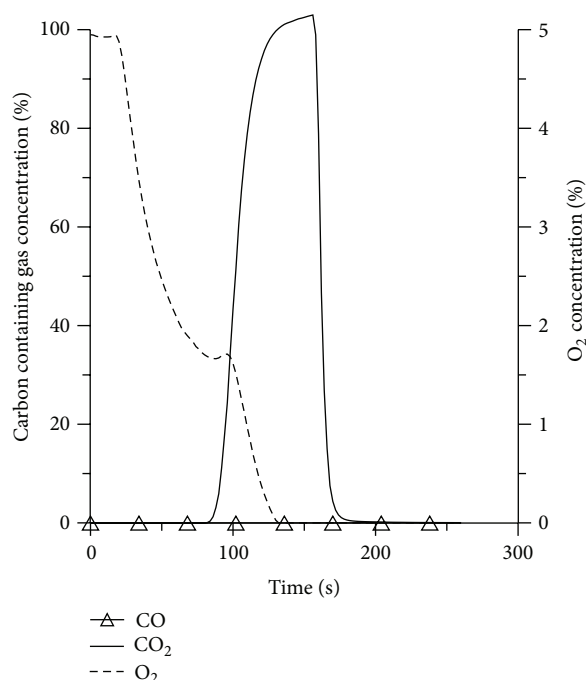
FIGURE 7: Dry gas concentration profile of the second syngas cycle at 950°C for the 5.6% MgO 1300 sample.

FIGURE 8: Syngas yield as a function of solid conversion for the second syngas cycle at 950°C.

represents the temperature after the 1050°C cycles. Decrease of the methane yield as a function of decreasing omega indicates that less methane was converted when the oxygen carrier was further reduced. Figure 10 summarizes the average methane yield at different temperatures for all samples along the temperature stair described in Section 3.4.2, with the exception of the last cycles at 950°C (2). The average γ_{CH4} is an average value of methane conversions of two reduction cycles operated at the same temperature.

The effect of temperature on the oxygen carriers' reactivity is clearly seen in the figures, especially from 900°C to 950°C. At 950°C, methane conversion of all the samples is already around 99%, making it hard to see the effect of further temperature change. The methane yield at 1000°C is a little bit lower than 950°C for the oxygen carrier 5.6% MgO 1300, but the difference is very small. Although high temperature improves methane conversion, it may cause deactivation in the oxygen carriers' reactivity. This was examined by comparing the reactivity at 950°C, before (1), and after (2) testing at the maximum temperature; see Figure 9(b). The particles reactivity at 950°C (1) (dashed and dotted lines) is apparently somewhat higher than the reactivity after the high temperature cycles (the dashed line). This indicates that materials suffer some deactivation, likely caused during the high temperature cycles. Some deactivation was seen for all investigated samples, as seen in Figure 10.

The ability of the oxygen carrier particles to release oxygen in the gas phase was also investigated at different temperatures. The results of the materials CLOU properties are summarized in Figures 11 and 12. The oxygen concentration profile presented in Figure 11 was similar to the other tested
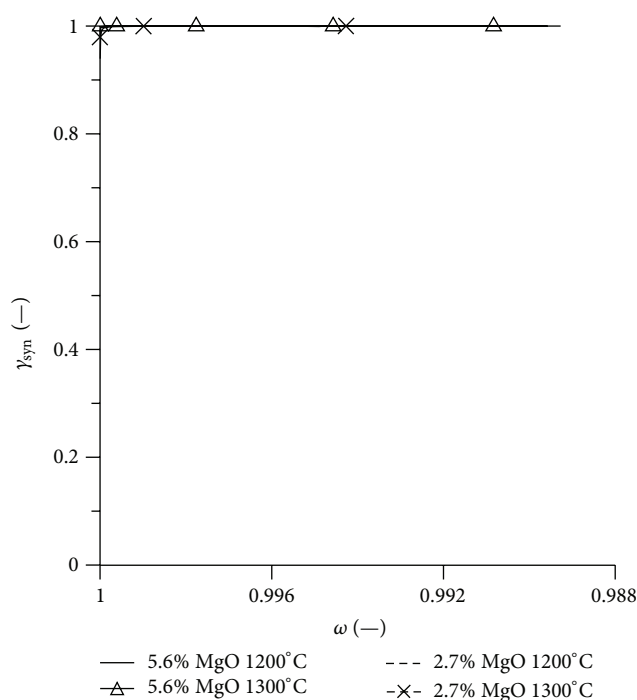
samples, with only small variations. For each inert cycle, the oxygen concentration at the end of 360 s was collected and shown as a function of temperature in Figure 12 for each investigated material.

As can be seen, operational temperature does not influence the materials CLOU properties in a significant way, although the particles release somewhat more oxygen as a function of temperature in the interval between 900°C and 950°C, and there is a drop at the highest temperature of 1050°C for all materials. The lower concentration of oxygen release for the 5.6% MgO 1300 sample at 950°C (2) cycles compared with the one at 950°C (1) indicates some deactivation of the material; see Figure 11(b). This was seen for all investigated particles; see Figure 12. The samples containing less MgO releases a little bit more oxygen at temperatures lower than 1050°C. The lower degree of oxygen release at the higher temperatures may be explained by the fact that the material is oxidized to a lesser extent at the higher temperatures [29, 31], meaning that the (3-δ) in reaction (5) decreases. This means that the oxygen capacity for the uncoupling reactions may decrease. The lower degree of oxygen release could also due to the formation of spinel, such as $CaMn_2O_4$, see discussion for further information.

4.4. Stability of Oxygen Carriers' Reactivity. To study the stability of the oxygen carrier, 50 short reduction cycles with methane were performed on 5.6% MgO 1300 particles. The reduction period was set to 2 s and 14 s to investigate the effect of reduction period length on the oxygen carriers' activity. Figure 13 shows the average methane conversion for 50 cycles at an operation temperature of 950°C. In both 2 s reduction
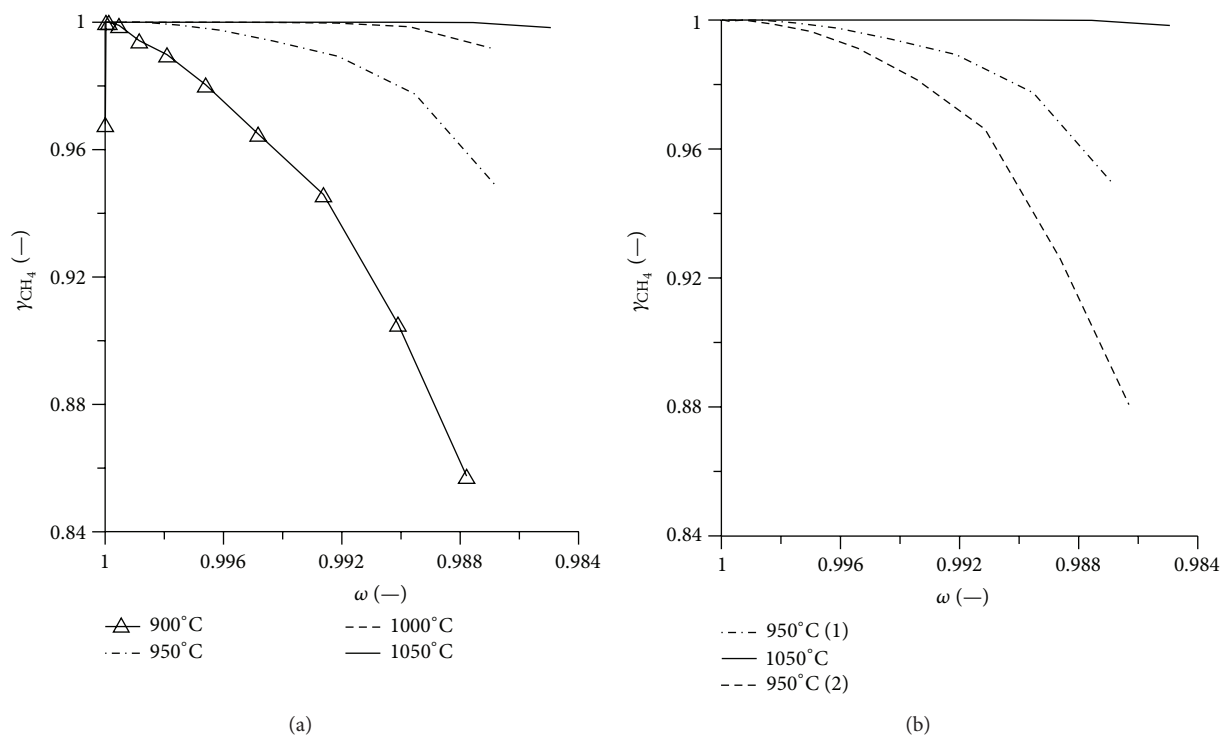
(a)

(b)

FIGURE 9: The methane yield as a function of solids conversion for 20 s reduction of 5.6% MgO 1300 oxygen carrier; (a) methane yield versus solid conversion for different temperatures and (b) the comparison of methane conversions at 950°C before and after 1050°C cycles. Data obtained from the second cycle is presented.
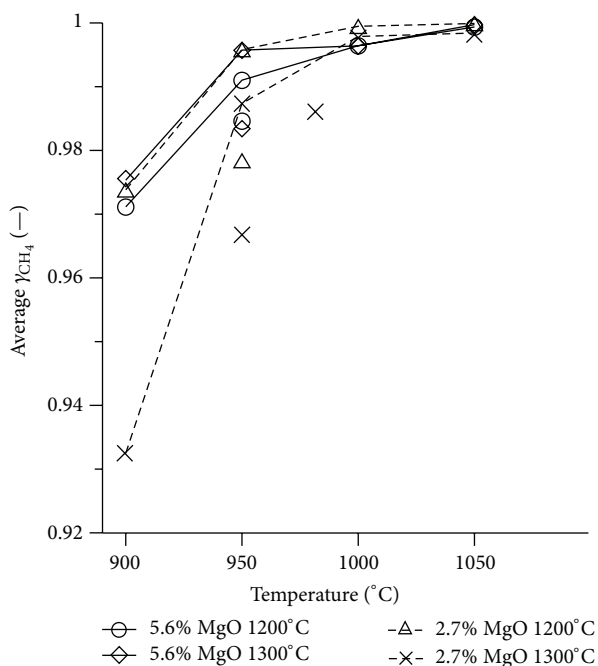

FIGURE 10: The average methane yield of 5.6% MgO and 2.7% MgO oxygen carriers as a function of temperature (data was selected for ω from 1 to 0.99). The single dots separated from the lines present the results at 950°C (2) cycles.

and 14 s reduction tests, the material's reactivity maintained well during 50 cycles, and a slight growth in reactivity is noticed. In stability test, less bed material (2 g) and higher methane flow (900 mL$_N$/min) were applied. The low methane conversion, in the range of 20%–50%, compared with full methane conversion in Sections 4.2 and 4.3, is reasonable.

4.5. Characterization of Oxygen Carriers. The morphology of 5.6% MgO 1300 particles was investigated by light microscopy and SEM. Figure 14 shows the light microscope pictures of fresh and used samples after 50 cycles. In Figure 14, the blue grids are 1 mm squares of the background millimeter paper. The images marked with (a) are fresh particles. The pictures marked with (b) and (c) exhibit the particles exposed to 2 s and 14 s methane reduction, respectively. Comparing the size of the particles, one can find that the particles after 14 s reduction cycles are somewhat bigger than other samples, while the difference between fresh and particles used for 2 s reduction cycles was quite small. This result may suggest that the oxygen carriers expand when reacting with methane.

The SEM pictures of fresh and used (after general reactivity test, cooled down in 5% O$_2$) 5.6% MgO 1300 particles are shown in Figure 15. The material maintains good spherical shape after experiments under different conditions. The cracks on some of the particles seen in the pictures were likely caused during the manufacture since they were found on fresh particles and on used ones. No obvious dust
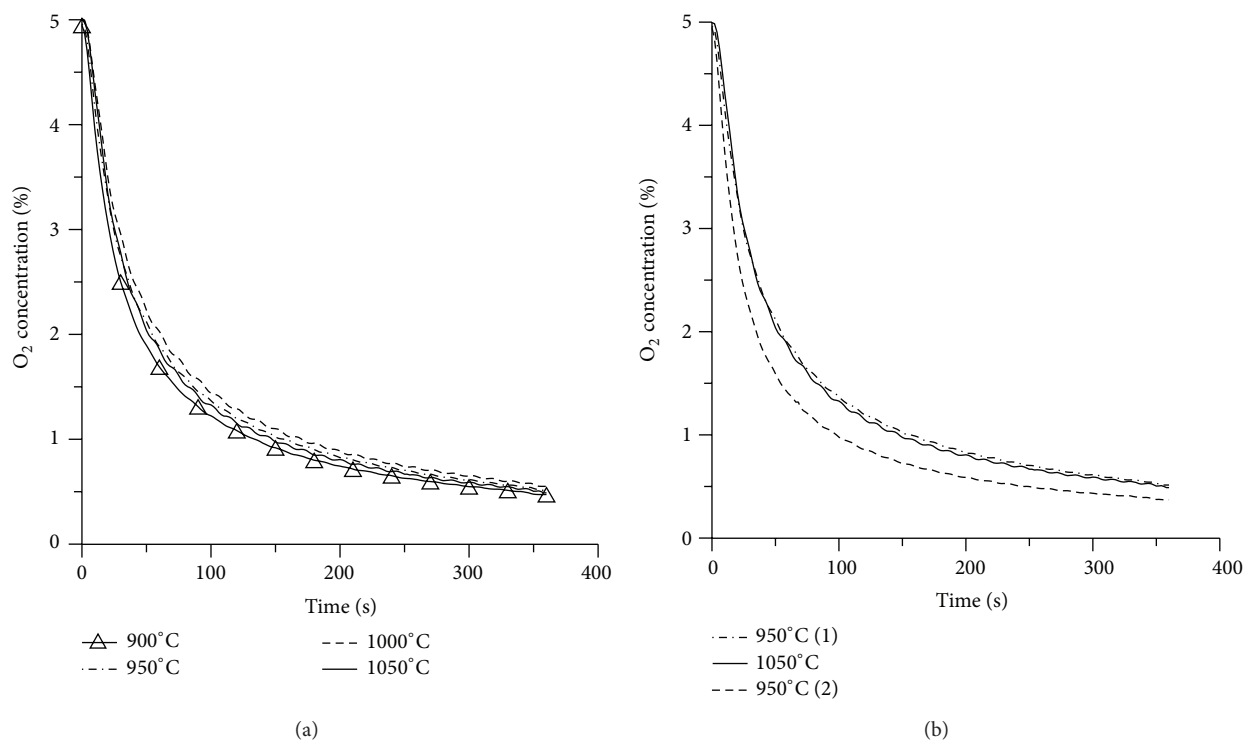
(a)

(b)

FIGURE 11: The O_2 concentration profile of inert cycles for the 5.6% MgO 1300 oxygen carrier; (a) oxygen concentration versus time as a function of temperature and (b) the comparison of oxygen profiles at 950°C before and after 1050°C cycles. Data obtained from the second conducted cycle is presented.
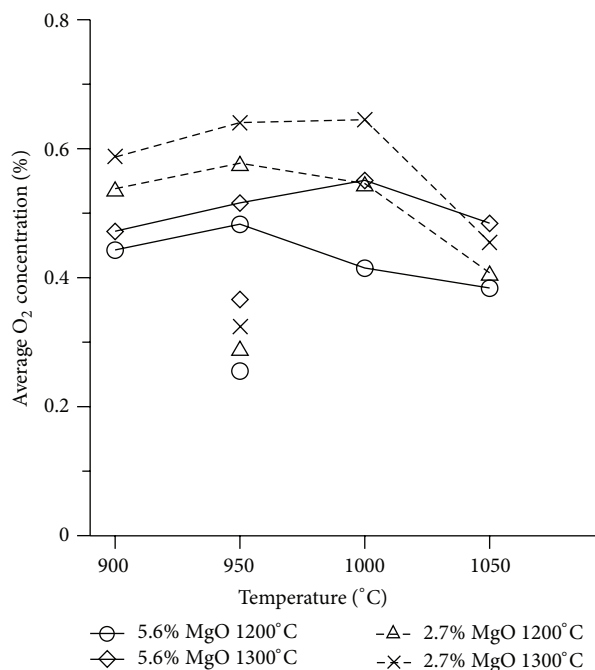

FIGURE 12: Released gaseous oxygen concentrations at the end of 360 s inert cycles by 5.6% MgO and 2.7% MgO oxygen carriers at different temperatures. The single dots separated from the lines present the results at 950°C (2) cycles.

formation was noticed during the experiments. On careful examination of the particle surface using energy-dispersive X-ray spectroscopy, it was discovered that there were many small heterogeneous inclusions on the surface which were identified as MgO. Hence, it does not appear that the MgO was included in the perovskite structure, rather the MgO seems to present mainly as a separate phase and in small grains.

The crystalline phases of the oxygen carriers are summarized in Table 7. Images were taken for fresh samples, used samples which were finished after inert cycle at 1000°C and cooled in 5% O_2, and used samples after reduction at 950°C and cooled in pure N_2. The phases for the used samples which were cooled in N_2 after the temperature stair were difficult to interpret due to low peak intensities of the XRD peaks. The crystalline phases are thus not provided for these samples. In the fresh samples, $CaMnO_{3-\delta}$ and MgO were identified in all samples. The multiple phases characterized match the EDX results, where free MgO was identified on the oxygen carrier particle surface. This confirms that MgO was not incorporated into the perovskite structure and hence the oxygen carriers consist of separated $CaMnO_{3-\delta}$ and MgO phases. In most cases, the same crystalline phases were identified in fresh particles and particles after tests which were removed after oxidation. This suggests that these $CaMnO_{3-\delta}$ materials have a good stability in the CLC process. The minor phase $CaMn_2O_4$ identified in used 5.6% MgO
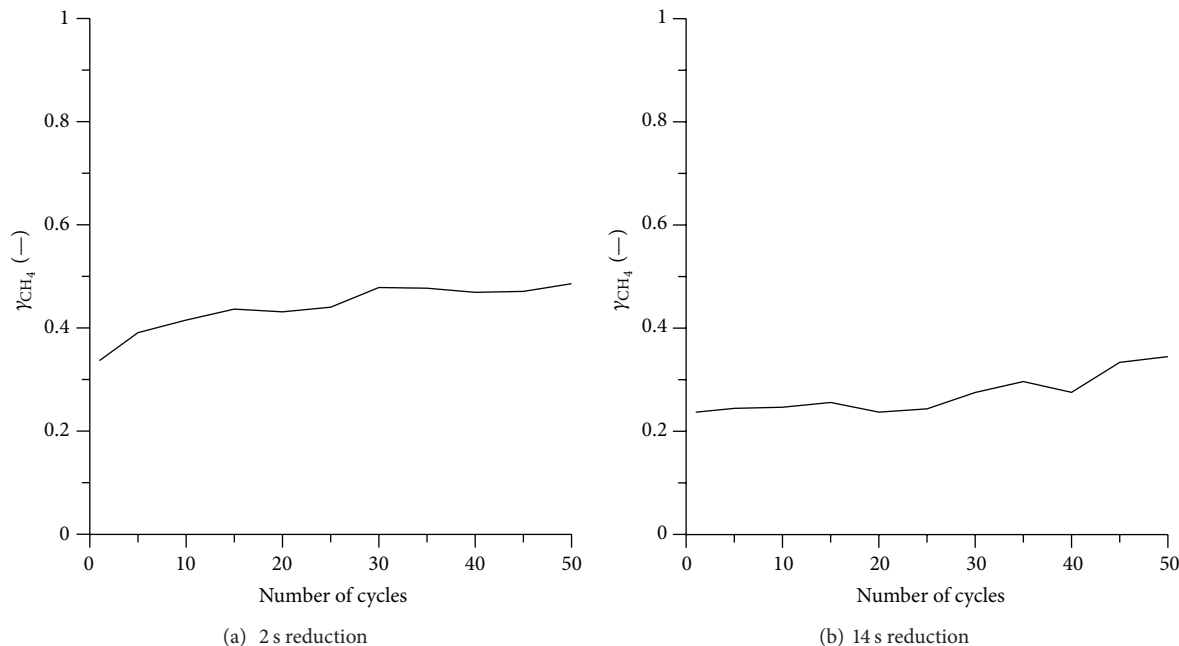
(a) 2 s reduction

(b) 14 s reduction

FIGURE 13: Methane conversion, (γ_{CH_4}) as a function of number of cycles for 5.6% MgO 1300 oxygen carrier.

TABLE 7: Crystalline phases identified in investigated samples.

Sample	Sintering temperature	Fresh	Used (cooled in 5% O_2)
5.6% MgO	1200°C	$CaMnO_{2.97}$, MgO	$CaMnO_{2.98}$, $CaMn_2O_4$, MgO
	1300°C	$CaMnO_{2.95}$, MgO	$CaMnO_{2.95}$, MgO
2.7% MgO	1200°C	$CaMnO_{2.95}$, MgO	$CaMnO_{2.95}$, MgO
	1300°C	$CaMnO_{2.95}$, MgO	$CaMnO_{2.95}$, MgO

1200 sample was reported as a decomposition product of $CaMnO_{3-\delta}$ at lower oxygen deficiency values [32]. Formation of a small amount of $CaMn_2O_4$ after the reactivity test could be reasonable considering the sample had been reduced with both methane and syngas. During preparation of the oxygen carrier particles, the molar ratio of calcium and manganese is higher than one. However, $CaMnO_{3-\delta}$ is the only XRD detected phase containing Ca and Mn. This means that the oxygen carriers should contain other calcium phases, such as CaO or $Ca_2MnO_{4-\delta}$, which were not identified by XRD. The reason could be that the amounts of other calcium phases are too low (<5 wt%) to be detected with the used apparatus; see below for further discussion.

5. Discussion

The perovskite $CaMn_xMg_{1-x}O_{3-\delta}$ studied in this work exhibited promising behavior with respect to parameters important for CLOU, that is, oxygen release, reactivity with methane, and syngas as well as fluidization properties. High reactivity towards methane in the range 93%–100% and full conversion of syngas were achieved at all examined temperatures. The particles have good fluidization properties, neither significant attrition nor agglomeration was observed. Though a slight deactivation was noticed following operation

at 1050°C, the materials still worked quite well when the temperature was reduced.

Previously, NiO has been the most promising oxygen carrier material for gas application [12, 37, 40]. Nevertheless, there are several problems with utilization of NiO as an oxygen carrier. Besides the high cost and toxicity, there is a thermodynamic limitation of the NiO/Ni system, which restricts methane to be fully converted to CO_2 and H_2O [11]. Several studies report around 1% CO in the exhausted stream from the fuel reactor when using NiO as an oxygen carrier [13, 14, 37].

The studied calcium manganite oxygen carriers were produced from cheap raw materials Mn_3O_4, $Ca(OH)_2$ and MgO using the commercial available spray-drying manufacturing method. As there are no thermodynamic limitation to convert fuel gas completely to CO_2 and H_2O, this type of material can clearly be a viable alternative to Ni-based material provided that the reactivity and stability are good. In this work, average methane conversion to CO_2 and H_2O of above 98% was achieved at temperatures of 950°C and above utilizing 57 kg/MW of CH_4; see Figure 10. This is comparable to the reactivity seen at similar conditions using spray-dried Ni-based materials [37]. And unlike NiO, neither unconverted methane at the beginning of fuel injection, at high oxidation levels of the oxygen carrier, nor CO at the
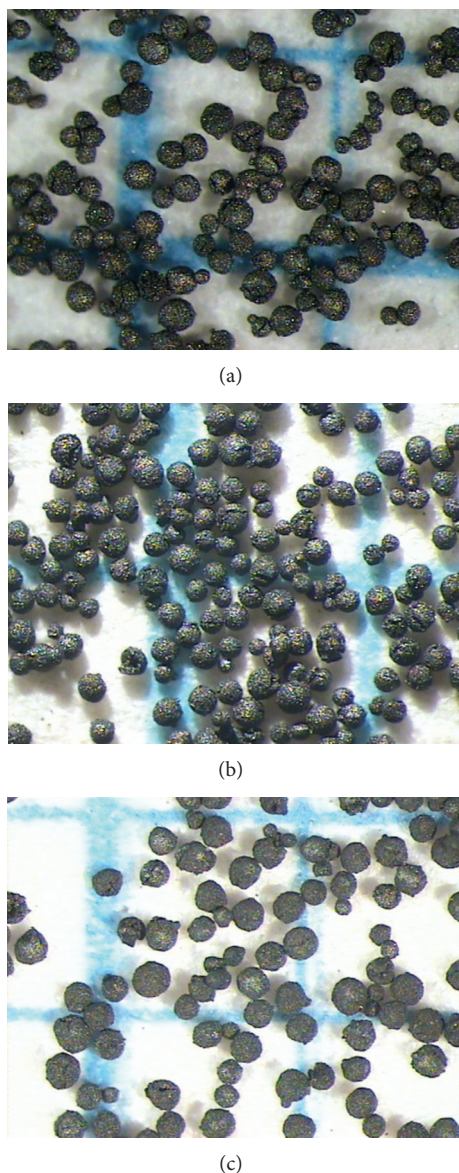
(a)

(b)

(c)

Figure 14: Light microscope pictures of 5.6% MgO 1300 particles both fresh and used after 50 cycles. (a) fresh particles; (b) particles on which 50 cycles of 2 s reduction was performed; (c) particles on which 50 cycles of 14 s reduction was performed.

end of the reduction period was observed. In the Chalmers 10 kW continuous system, when using the $CaMn_{0.9}Mg_{0.1}O_3$ as oxygen carrier, 100% methane was fully converted to CO_2 and H_2O above 900°C, and more than 1% O_2 was detected in the outlet stream of the fuel reactor [36]. This suggests that gaseous reaction between O_2 and CH_4 is the main reaction mechanism in the fuel reactor. This is in contrast to NiO, which is a CLC material, meaning that the direct gas-solid reaction is the main mechanism for fuel conversion.

The oxygen deficiency δ in $CaMnO_{3-\delta}$ is a function of oxygen partial pressure and temperature. Leonidova et al. [31] and Goldyreva et al. [41] studied the oxygen deficiency under different conditions and provided a phase diagram

of $CaMnO_{3-\delta}$ where δ was a function of oxygen partial pressure at different temperatures. At a fixed temperature, δ increases with decreasing oxygen partial pressure meaning that more oxygen is released under lower oxygen partial pressure environment. Conversely, at a constant partial pressure of oxygen, δ increases with temperature. This indicates that $CaMnO_{3-\delta}$ oxygen carriers may not be oxidized to the same level at higher temperatures as it would be at lower temperatures. Despite this fact, the amount of oxygen that is available for CLOU depends on the δ difference between the oxidized and reduced form of $CaMnO_{3-\delta}$. Though oxidized $CaMnO_{3-\delta}$ has less oxygen at higher temperature, it may be reduced further at low partial pressures of O_2, as would be existing in the fuel reactor of a chemical-looping unit [31, 41]. For instance, for an oxygen partial pressure change, from 0.05 atm to 0.005 atm, the oxygen carrier $CaMnO_{3-\delta}$ should release approximately the same amount of oxygen at higher and lower temperature cases employed in this work. This matches the experimental results well, where the oxygen carriers' oxygen capacity seemed to be similar independent of temperature. On the other hand, the growth of oxygen carrier reactivity towards CH_4 with temperature may due to an increase of oxygen release rate as a function of temperature.

The level of oxygen deficiency of $CaMnO_{3-\delta}$ cannot grow infinitely, and seems to be limited by the decomposition of $CaMnO_{3-\delta}$ to $CaMn_2O_4$ and $Ca_2MnO_{4-\delta}$ [32]. The reported boundary $3-\delta$ value was within the range of 2.863 to 2.83 for temperature interval 950°C to 1050°C. Beyond the boundary level, further removing of oxygen triggered the decomposition of $CaMnO_{3-\delta}$. However, this decomposition process was reversible and very slow even at 1000°C [32]. For $CaMnO_{3-\delta}$ oxygen carriers applied in a CLC process where typical solid conversion changes could be around 1 wt%; this leads to the $3-\delta$ value above 2.86, assuming fully oxidized sample from the air reactor. Hence, in order to avoid decomposition products and fully utilize the perovskites uncoupling properties, it may be a good idea to avoid deep reduction of the oxygen carrier in a real system and to keep the change in the mass based conversion level below 1% if possible. This could be achieved by employing high circulation of particles between the reactors. Another option to extract more oxygen from the material is to employ a lower temperature in the air reactor compared to the fuel reactor, something which should be feasible considering that the overall reactions should be exothermic in the fuel reactor [29]. The small amount of detected $CaMn_2O_4$ in the used 5.6% MgO 1200°C sample is likely due to the described decomposition process. It should be noted, however, that the identified phase had a very low intensity and is thus likely present in rather small amounts. Further, it is possible that also the other used samples contained this phase, but in undetectable quantities. Even in well controlled solid state chemistry synthesis processes, small amount of $CaMn_2O_4$ was also discovered as a secondary phase together with the $CaMnO_{3-\delta}$ [42–44].

The perovskite $CaMnO_{3-\delta}$ can exist as different structures, depending upon temperature and partial pressure of oxygen. When heating in air, stoichiometry $CaMnO_3$ with orthorhombic structure at room temperature lost oxygen forming the nonstoichiometric $CaMnO_{3-\delta}$ and transforms to
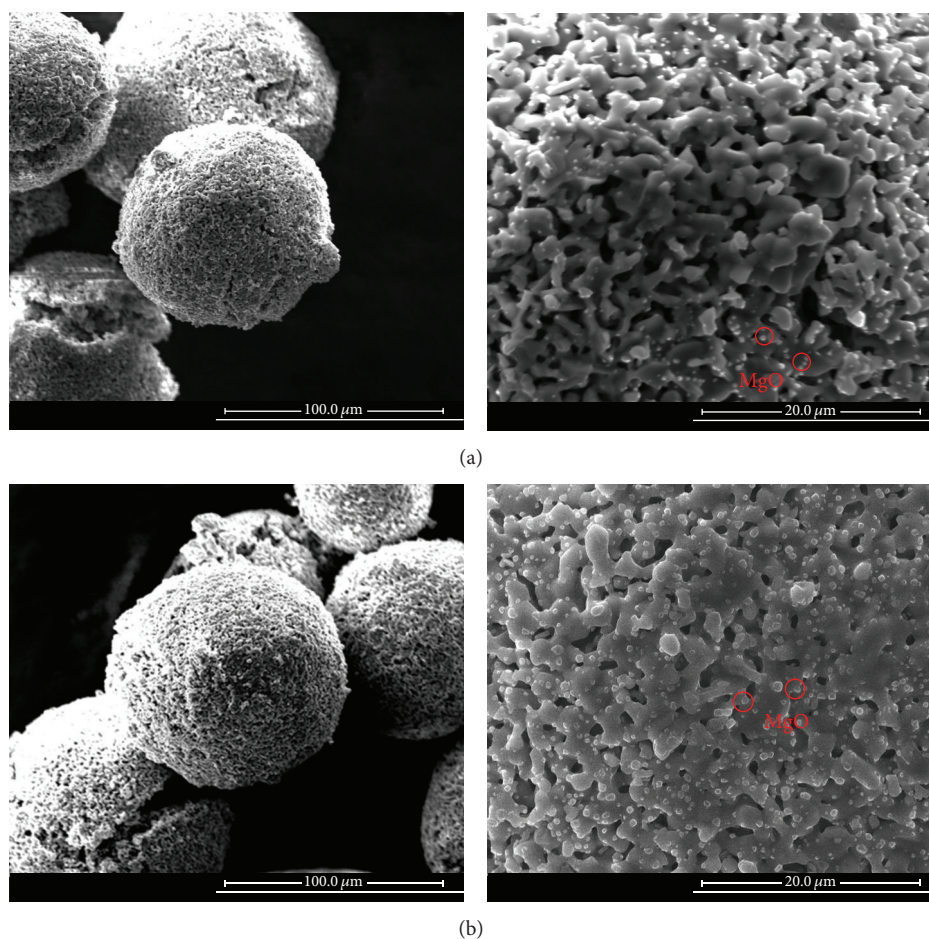
(a)

(b)

FIGURE 15: SEM image of 5.6% MgO 1300 sample. (a) Fresh sample. (b) Used sample (cooled down to room temperature by 5% O_2 in N_2).

tetragonal and subsequently to cubic symmetry structure at 869°C and 913°C [31, 45–47]. This transition would happen at lower temperatures in our experiment since the particles were heated in 5% O_2 in N_2 under a much lower oxygen partial pressure compared to air. Such structure transitions involve changes of crystalline lattice parameters, although the compounds have the same chemical stoichiometry. During isothermal cycling in the fuel reactor at temperatures above 900°C, the cubic structure should be the most stable. However, it is possible that phase changes can occur during heating and cooling of the particles. In the current experiment, no degradation of particles was seen; so although there could have been certain structure transformations, as described above, these do not seem to have affected the physical integrity of the particles to any appreciable extent. In addition, the long-term testing in continuous operation of this type of particles without major attrition also suggests that possible degradation due to phase transformations should not be a major issue [36].

For the investigated particles the moles of Ca is greater than the moles of Mn. However, only $CaMnO_{3-\delta}$ and MgO were identified, meaning that Ca should be present in additional phases. The highly possible phases which contain Ca could be CaO or $Ca_2MnO_{4-\delta}$. Horowitz and Longo suggested

that CaO and $CaMnO_3$ were the phases in Ca-Mn-O system at temperature below 1300°C when the Ca to Mn molar ratio was above 1, and the oxygen partial pressure 0.2 atm [48]. On the other hand, several research groups identified small amount of $CaMn_2O_4$ which coexited with $CaMnO_{3-\delta}$ during synthesis of $CaMnO_{3-\delta}$ when using stoichiometric molar amount of Ca and Mn during production. Since $CaMn_2O_4$ and $Ca_2MnO_{4-\delta}$ are the decomposition products of $CaMnO_{3-\delta}$ [32], $Ca_2MnO_{4-\delta}$ may be present in the oxygen carrier particles as well, but in amounts too small to be detected by the present XRD unit. From characterization, it is clear that Mg is not incorporated into the perovskite structure, and this is likely due to the low ionic radii of Mg [49]. This is unlike the cations Fe and Ti, which can substitute Mn in the perovskite structure [50, 51]. Still, in a prior investigation, Hallberg et al. [35] clearly showed that the calcium manganite with Mg addition had better behavior with respect to CLOU than material doped with Fe and Ti. This suggests that MgO may be an active component in the oxidation reaction with methane; for instance, it may have a role as a reforming catalyst on the particle exterior. To clarify the role of MgO and $CaMnO_{3-\delta}$ in methane conversion reaction, further investigation of the mechanism is apparently needed. On the other hand, considering the encouraging

results reported here, by Hallberg et al. and Källén et al. in both batch and $10\,kW_{th}$ gas-fired CLC unit on the same type of material [35, 36], it is quite clear that this oxygen carrier is a valid alternative to NiO.

6. Conclusion

Cheap and environmentally friendly Ca-Mn combined oxide particles with general formula $CaMn_xMg_{1-x}O_3$ were produced using the spray-drying method. The active compound in the oxygen carriers was likely the perovskite material $CaMnO_{3-\delta}$, and it showed highly promising results with respect to reactivity and stability. Generally, the methane and syngas conversion was high, and the particles exhibited oxygen uncoupling at all investigated temperatures in the range $900–1050°C$. There was some deactivation of the particles, especially prominent after exposure to fuel at high temperature, $1050°C$. $CaMn_{0.8}Mg_{0.2}O_3$ sintered at $1300°C$ showed good stability in 50 cycles' tests, and even a small increase in reactivity was noted.

Acknowledgment

References

[1] IEA, *CO₂ Emissions From Fuel Combustion 2012*, OECD Publishing, Paris, France, 2012.

[2] IPCC, *Carbon Dioxide Capture and Storage*, IPCC, Geneva, Switzerland, 2005.

[3] A. Lyngfelt, "Oxygen carriers for chemical looping combustion −4000 h of operational experience," *Oil and Gas Science and Technology*, vol. 66, no. 2, pp. 161–172, 2011.

[4] J. Adanez, A. Abad, F. Garcia-Labiano, P. Gayan, and L. F. de Diego, "Progress in chemical-looping combustion and reforming technologies," *Progress in Energy and Combustion Science*, vol. 38, no. 2, pp. 215–282, 2012.

[5] M. Ishida and H. Jin, "A novel chemical-looping combustor without NOx formation," *Industrial and Engineering Chemistry Research*, vol. 35, no. 7, pp. 2469–2472, 1996.

[6] A. Lyngfelt, B. Leckner, and T. Mattisson, "A fluidized-bed combustion process with inherent CO₂ separation; application of chemical-looping combustion," *Chemical Engineering Science*, vol. 56, no. 10, pp. 3101–3113, 2001.

[7] B. Kronberger, E. Johansson, G. Löffer, T. Mattisson, A. Lyngfelt, and H. Hofbauer, "A two-compartment fluidized bed reactor for CO₂ capture by chemical-looping combustion," *Chemical Engineering and Technology*, vol. 27, no. 12, pp. 1318–1326, 2004.

[8] T. Mattisson, A. Lyngfelt, and H. Leion, "Chemical-looping with oxygen uncoupling for combustion of solid fuels," *International Journal of Greenhouse Gas Control*, vol. 3, no. 1, pp. 11–19, 2009.

[9] M. Ishida, D. Zheng, and T. Akehata, "Evaluation of a chemical-looping-combustion power-generation system by graphic exergy analysis," *Energy*, vol. 12, no. 2, pp. 147–154, 1987.

[10] T. Mattisson and A. Lyngfelt, "Capture of CO₂ using chemical-looping combustion," in *Proceedings of the 1st Biennial Meeting of the Scandinavian-Nordic Section of the Combustion Institute*, Göteborg, Sweden, April 2001.

[11] E. Jerndal, T. Mattisson, and A. Lyngfelt, "Thermal analysis of chemical-looping combustion," *Chemical Engineering Research and Design*, vol. 84, no. 9, pp. 795–806, 2006.

[12] C. Linderholm, T. Mattisson, and A. Lyngfelt, "Long-term integrity testing of spray-dried particles in a 10-kW chemical-looping combustor using natural gas as fuel," *Fuel*, vol. 88, no. 11, pp. 2083–2096, 2009.

[13] P. Kolbitsch, J. Bolhàr-Nordenkampf, T. Pröll, and H. Hofbauer, "Operating experience with chemical looping combustion in a 120 kW dual circulating fluidized bed (DCFB) unit," *International Journal of Greenhouse Gas Control*, vol. 4, no. 2, pp. 180–185, 2010.

[14] T. Mattisson, M. Johansson, and A. Lyngfelt, "The use of NiO as an oxygen carrier in chemical-looping combustion," *Fuel*, vol. 85, no. 5-6, pp. 736–747, 2006.

[15] I. Adanez-Rubio, P. Gayan, A. Abad, L. F. de Diego, F. Garcia-Labiano, and J. Adanez, "Evaluation of a spray-dried CuO/MgAl₂O4 oxygen carrier for the chemical looping with oxygen uncoupling process," *Energy & Fuels*, vol. 5, no. 26, pp. 3069–3081, 2012.

[16] P. Gayán, I. Adánez-Rubio, A. Abad, L. F. de Diego, F. García-Labiano, and J. Adánez, "Development of Cu-based oxygen carriers for chemical-looping with oxygen uncoupling (CLOU) process," *Fuel*, vol. 96, no. 1, pp. 226–238, 2012.

[17] M. Arjmand, A. Azad, H. Leion, A. Lyngfelt, and T. Mattisson, "Prospects of Al₂O₃ and MgAl₂O₄-supported CuO oxygen carriers in chemical-looping combustion (CLC) and chemical-looping with oxygen uncoupling (CLOU)," *Energy & Fuels*, vol. 25, no. 11, pp. 5493–5502, 2011.

[18] A. Abad, I. Adánez-Rubio, P. Gayán, F. García-Labiano, L. F. de Diego, and J. Adánez, "Demonstration of chemical-looping with oxygen uncoupling (CLOU) process in a 1.5 kW(th) continuously operating unit using a Cu-based oxygen-carrier," *International Journal of Greenhouse Gas Control*, vol. 6, pp. 189–200, 2012.

[19] L. F. de Diego, F. García-Labiano, P. Gayán, J. Celaya, J. M. Palacios, and J. Adánez, "Operation of a 10 kWth chemical-looping combustor during 200 h with a CuO-Al₂O₃ oxygen carrier," *Fuel*, vol. 86, no. 7-8, pp. 1036–1045, 2007.

[20] T. Mattisson, A. Järdnäs, and A. Lyngfelt, "Reactivity of some metal oxides supported on alumina with alternating methane and oxygen—application for chemical-looping combustion," *Energy & Fuels*, vol. 17, no. 3, pp. 643–651, 2003.

[21] P. Cho, T. Mattisson, and A. Lyngfelt, "Comparison of iron-, nickel-, copper- and manganese-based oxygen carriers for chemical-looping combustion," *Fuel*, vol. 83, no. 9, pp. 1215–1225, 2004.

[22] L. F. de Diego, P. Gayán, F. García-Labiano, J. Celaya, A. Abad, and J. Adánez, "Impregnated CuO/Al₂O₃ oxygen carriers for chemical-looping combustion: avoiding fluidized bed agglomeration," *Energy & Fuels*, vol. 19, no. 5, pp. 1850–1856, 2005.

[23] Q. Zafar, A. Abad, T. Mattisson, B. Gevert, and M. Strand, "Reduction and oxidation kinetics of Mn₃O₄/Mg-ZrO₂ oxygen carrier particles for chemical-looping combustion," *Chemical Engineering Science*, vol. 62, no. 23, pp. 6556–6567, 2007.

[24] G. Azimi, H. Leion, T. Mattisson, and A. Lyngfelt, "Chemical-looping with oxygen uncoupling for Mn-based materials, testing in batch fluidized bed," in *Proceedings of the 10th International Conference on Greenhouse Gas Control Technologies*, Amsterdam, The Netherlands, September 2010.

[25] G. Azimi, M. Rydén, H. Leion, T. Mattisson, and A. Lyngfelt, "(Mn$_z$Fe$_{1-z}$)$_y$O$_x$ combined oxides as oxygen carrier for chemical-looping with oxygen uncoupling," *AIChE Journal*, vol. 2, no. 59, pp. 582–588, 2013.

[26] M. Rydén, A. Lyngfelt, and T. Mattisson, "Combined manganese/iron oxides as oxygen carrier for chemical looping combustion with oxygen uncoupling (CLOU) in a circulating fluidized bed reactor system," *Energy Procedia*, no. 4, pp. 341–348, 2011.

[27] A. Shulman, E. Cleverstam, T. Mattisson, and A. Lyngfel, "Manganese/iron, manganese/nickel, and manganese/silicon oxides used in chemical-looping with oxygen uncoupling (CLOU) for combustion of methane," *Energy & Fuels*, vol. 23, no. 10, pp. 5269–5275, 2009.

[28] D. Jing, E. Y. S. Hermans, H. Leion, M. Rydén, T. Mattisson, and A. Lyngfelt, "Manganese silica combined oxide as oxygen carrier for chemical-looping combustion," in *Proceedings of the 2nd International Conference on Chemical Looping*, pp. 26–28, Darmstadt, Germany, September 2012.

[29] M. Rydén, H. Leion, T. Mattisson, and A. Lyngfelt, "Combined oxides as oxygen-carrier material for chemical-looping with oxygen uncoupling," *Applied Energy*. In press.

[30] T. Mattisson, "Materials for chemical-looping with oxygen uncoupling," *ISRN Chemical Engineering*, vol. 2013, Article ID 526375, 19 pages, 2013.

[31] E. I. Leonidova, I. A. Leonidov, M. V. Patrakeev, and V. L. Kozhevnikov, "Oxygen non-stoichiometry, high-temperature properties, and phase diagram of CaMnO$_{3-\delta}$," *Journal of Solid State Electrochemistry*, vol. 15, no. 5, pp. 1071–1075, 2011.

[32] E. Bakken, T. Norby, and S. Stølen, "Nonstoichiometry and reductive decomposition of CaMnO$_{3-\delta}$," *Solid State Ionics*, vol. 176, no. 1-2, pp. 217–223, 2005.

[33] H. Leion, Y. Larring, E. Bakken, R. Bredesen, T. Mattisson, and A. Lyngfelt, "Use of CaMn$_{0.875}$Ti$_{0.125}$O$_3$ as oxygen carrier in chemical-looping with oxygen uncoupling," *Energy & Fuels*, vol. 23, no. 10, pp. 5276–5283, 2009.

[34] M. Rydén, A. Lyngfelt, and T. Mattisson, "CaMn$_{0.875}$Ti$_{0.125}$O$_3$ as oxygen carrier for chemical-looping combustion with oxygen uncoupling (CLOU)—experiments in a continuously operating fluidized-bed reactor system," *International Journal of Greenhouse Gas Control*, vol. 5, no. 2, pp. 356–366, 2011.

[35] P. Hallberg, D. Jing, M. Rydén, T. Mattisson, and A. Lyngfelt, "Chemical looping combustion and chemical looping with oxygen uncoupling experiments in a batch reactor using spray-dried CaMn$_{1-x}$M$_x$O$_{3-\delta}$ (M = Ti, Fe, Mg) particles as oxygen carriers," *Energy & Fuels*, vol. 3, no. 27, pp. 1473–1481, 2013.

[36] M. Källén, M. Rydén, C. Dueso, T. Mattisson, and A. Lyngfelt, "CaMn$_{0.9}$Mg$_{0.1}$O$_{3-\delta}$ as oxygen carrier in a gas-fired 10 kWthchemical-looping combustion unit," *Industrial & Engineering Chemistry Research*, vol. 21, no. 52, pp. 6923–6932, 2013.

[37] E. Jerndal, T. Mattisson, and A. Lyngfelt, "Investigation of different NiO/NiAl$_2$O$_4$ particles as oxygen carriers for chemical-looping combustion," *Energy & Fuels*, vol. 23, no. 2, pp. 665–676, 2009.

[38] S. Sundqvist, H. Leion, M. Rydén, A. Lyngfelt, and T. Mattisson, "CaMn$_{0.875}$Ti$_{0.125}$O$_{3-\delta}$ as an oxygen carrier for chemical-looping with oxygen uncoupling (CLOU)-solid-fuel testing and sulfur interaction," *Energy Technology*, vol. 5-6, no. 1, pp. 338–344, 2013.

[39] E. Jerndal, H. Leion, L. Axelsson et al., "Using low-cost iron-based materials as oxygen carriers for chemical looping combustion," *Oil and Gas Science and Technology*, vol. 66, no. 2, pp. 235–248, 2011.

[40] J. Bolhàr-Nordenkampf, T. Pröll, P. Kolbitsch, and H. Hofbauer, "Performance of a NiO-based oxygen carrier for chemical looping combustion and reforming in a 120 kW unit," in *Proceedings of the 9th International Conference on Greenhouse Gas Control Technologies*, vol. 1, pp. 19–25, November 2009.

[41] E. I. Goldyreva, I. A. Leonidov, M. V. Patrakeev, and V. L. Kozhevnikov, "Oxygen non-stoichiometry and defect equilibria in CaMnO$_{3-\delta}$," *Journal of Solid State Electrochemistry*, vol. 16, no. 3, pp. 1187–1191, 2012.

[42] E. Bakken, J. Boerio-Goates, T. Grande et al., "Entropy of oxidation and redox energetics of CaMnO$_{3-\delta}$," *Solid State Ionics*, vol. 176, no. 29-30, pp. 2261–2267, 2005.

[43] L. Rørmark, A. B. Mørch, K. Wiik, S. Stølen, and T. Grande, "Enthalpies of oxidation of CaMnO$_{3-\delta}$, Ca$_2$MnO$_{4-\delta}$ and SrMnO$_{3-\delta}$—deduced redox properties," *Chemistry of Materials*, vol. 13, no. 11, pp. 4005–4013, 2001.

[44] L. Bocher, M. H. Aguirre, R. Robert et al., "High-temperature stability, structure and thermoelectric properties of phases," *Acta Materialia*, vol. 57, no. 19, pp. 5667–5680, 2009.

[45] H. Taguchi, M. Nagao, T. Sato, and M. Shimada, "High-temperature phase transition of CaMnO$_{3-\delta}$," *Journal of Solid State Chemistry*, vol. 78, no. 2, pp. 312–315, 1989.

[46] L. Rormark, K. Wiik, S. Stolen, and T. Grande, "Oxygen stoichiometry and structural properties of La$_{1-x}$A$_x$MnO$_{3\pm\delta}$ (A = Ca or Sr and $0 \le x \le 1$)," *Journal of Materials Chemistry*, vol. 4, no. 12, pp. 1058–1067, 2002.

[47] K. R. Poeppelmeier, M. E. Leonowicz, J. C. Scanlon, J. M. Longo, and W. B. Yelon, "Structure determination of CaMnO$_3$ and CaMnO$_{2.5}$ by X-ray and neutron methods," *Journal of Solid State Chemistry*, vol. 45, no. 1, pp. 71–79, 1982.

[48] H. S. Horowitz and J. M. Longo, "Phase relations in the CaMnO system," *Materials Research Bulletin*, vol. 13, no. 12, pp. 1359–1369, 1978.

[49] C. Li, K. C. K. Soh, and P. Wu, "Formability of ABO$_3$ perovskites," *Journal of Alloys and Compounds*, vol. 372, no. 1-2, pp. 40–48, 2004.

[50] Neetika, A. Das, I. Dhiman et al., "Transport and magnetic properties of Fe doped CaMnO$_3$," *Journal of Applied Physics*, vol. 12, no. 112, Article ID 123913, 6 pages, 2012.

[51] K. Nakade, K. Hirota, M. Kato, and H. Taguchi, "Effect of the Mn^{3+} ion on electrical and magnetic properties of orthorhombic perovskite-type Ca(Mn$_{1-x}$Ti$_x$)O$_{3-\delta}$," *Materials Research Bulletin*, vol. 42, no. 6, pp. 1069–1076, 2007.